NOAA Technical Report NESDIS 49

Implementation of Reflectance Models in Operational AVHRR Radiation Budget Processing

Washington, D.C.
February 1990

U.S. DEPARTMENT OF COMMERCE
National Oceanic and Atmospheric Administration
National Environmental Satellite, Data, and Information Service

NOAA TECHNICAL REPORTS

National Environmental Satellite, Data, and Information Service

The National Environmental Satellite, Data, and Information Service (NESDIS) manages the Nation's civil Earth-observing satellite systems, as well as global national data bases for meteorology, oceanography, geophysics, and solar-terrestrial sciences. From these sources, it develops and disseminates environmental data and information products critical to the protection of life and property, national defense, the national economy, energy development and distribution, global food supplies, and the development of natural resources.

Publication in the NOAA Technical Report series does not preclude later publication in scientific journals in expanded or modified form. The NESDIS series of NOAA Technical Reports is a continuation of the former NESS and EDIS series of NOAA Technical Reports and the NESC and EDS series of Environmental Science Services Administration (ESSA) Technical Reports.

A limited number of copies are available by contacting Nancy Everson, NOAA/NESDIS, E/RA22, 5200 Auth Road, Washington, DC, 20233. Copies can also be ordered from the National Technical Information Service (NTIS), U.S. Department of Commerce, Sills Bldg., 5285 Port Royal Road, Springfield, VA. 22161, (703) 487-4650 (prices on request for paper copies or microfiche, please refer to PB number when ordering). A partial listing of more recent reports appear below:

NESDIS 1 Satellite Observations on Variations in Southern Hemisphere Snow Cover. Kenneth F. Dewey and Richard Heim, Jr., June 1983. (PB83 252908)

NESDIS 2 NODC 1 An Environmental Guide to Ocean Thermal Energy Conversion (OTEC) Operations in the Gulf of Mexico. National Oceanographic Data Center, June 1983. (PB84 115146)

NESDIS 3 Determination of the Planetary Radiation Budget from TIROS-N Satellites. Arnold Gruber, Irwin Ruff and Charles Earnest, August 1983. (PB84 100916)

NESDIS 4 Some Applications of Satellite Radiation Observations to Climate Studies. T.S. Chen, George Ohring and Haim Ganot, September 1983. (PB84 108109)

NESDIS 5 A Statistical Technique for Forecasting Severe Weather from Vertical Soundings by Satellite and Radiosonde. David L. Keller and William L. Smith, June 1983. (PB84 114099)

NESDIS 6 Spatial and Temporal Distribution of Northern Hemisphere Snow Cover. Burt J. Morse and Chester F. Ropelewski (NWS), October 1983. (PB84 118348)

NESDIS 7 Fire Detection Using the NOAA--Series Satellites. Michael Matson, Stanley R. Schneider, Billie Aldridge and Barry Satchwell (NWS), January 1984. (PB84 176890)

NESDIS 8 Monitoring of Long Waves in the Eastern Equatorial Pacific 1981-83 Using Satellite Multi-Channel Sea Surface Temperature Charts. Richard Legeckis and William Pichel, April 1984. (PB84 190487)

NESDIS 9 The NESDIS-SEL Lear Aircraft Instruments and Data Recording System. Gilbert R. Smith, Kenneth O. Hayes, John S. Knoll and Robert S. Koyanagi, June 1984. (PB84 219674)

NESDIS 10 Atlas of Reflectance Patterns for Uniform Earth and Cloud Surfaces (NIMBUS-7 ERB--61 Days). V.R. Taylor and L.L. Stowe, July 1984. (PB85 12440)

NESDIS 11 Tropical Cyclone Intensity Analysis Using Satellite Data. Vernon F. Dvorak, September 1984. (PB85 112951)

NESDIS 12 Utilization of the Polar Platform of NASA's Space Station Program for Operational Earth Observations. John H. McElroy and Stanley R. Schneider, September 1984. (PB85 1525027AS)

NESDIS 13 Summary and Analyses of the NOAA N-ROSS/ERS-1 Environmental Data Development Activity. John W. Sherman III, February 1984. (PB85 222743/43)

NESDIS 14 NOAA N-ROSS/ERS-1 Environmental Data Development (NNEEDD) Activity. John W. Sherman III, February 1985. (PB86 139284 A/S)

NESDIS 15 NOAA N-ROSS/ERS-1 Environmental Data Development (NNEEDD) Products and Services. Franklin E. Kniskern, February 1985, (PB86 213527/AS)

NESDIS 16 Temporal and Spatial Analyses of Civil Marine Satellite Requirements. Nancy J. Hooper and John W. Sherman III, February 1985. (PB86 212123/AS)

NESDIS 17 reserved

NOAA Technical Report NESDIS 49

Implementation of Reflectance Models in Operational AVHRR Radiation Budget Processing

V. Ray Taylor
Offfice of Research and Applications
Atmospheric Sciences Branch

Washington, D.C.
February 1990

U.S. DEPARTMENT OF COMMERCE
Robert A. Mosbacher, Secretary

National Oceanic and Atmospheric Administration
John A. Knauss, Under Secretary

National Environmental Satellite, Data, and Information Service
Thomas N. Pyke, Jr. , Assistant Administrator

Contents

List of Figures

Introduction

A major parameter in calculating the Earth's radiation budget is reflection by the illuminated Earth-atmosphere system. Data from Advanced Very High Resolution Radiometer (AVHRR) instruments on the NOAA satellite series have long been used to derive reflected radiation budget parameters. However, the accuracy of such estimates from narrow-band instruments has been challenged because of necessary but inaccurate assumptions.

To derive reliable reflectance parameters from AVHRR, one must, in an operational environment, convert an instantaneous, highly directional, narrowband radiation measurement into an estimate of daily average broadband flux over the whole upward hemisphere. This conversion is accomplished by applying models of the following types:

(1) Bi-directional (Solar zenith, Satellite zenith, relative azimuth angles) - This is a set of patterns, each valid for a particular interval of solar zenith angle and for an individual scene type. Each pattern shows the relative brightness as a function of the direction from which the scene is viewed.

(2) Directional (Solar Zenith Angle) - The relationship between albedo and solar zenith angle for a given scene type. This relationship can also be used to show the variation of albedo with time of day.

(3) Narrow to Broadband - A weighted combination of albedos or radiances from narrow band channels to yield an estimate of the broadband value. The weights used may also optimally be a function of scene type.

The term 'scene type' in the foregoing implies the necessity of invoking an additional 'model'.

(4) Scene Type Identification - classification of observations into a finite set of surface types for which the above models are available.

Prior to May, 1988 and in the absence of reliable models of the types listed above, the derivation of AVHRR short-wave radiation budget parameters (albedo, reflected flux, absorbed solar energy) included four assumptions which were known to be deficient. First was the assumption of isotropy in which a scene would appear equally bright regardless of viewing direction. Second was the assumption that the albedo of a viewed surface did not vary with the illumination (solar zenith) angle. This is the same as assuming that the instantaneous albedo of each observation is equal to the average daily albedo for that scene. Third, it was assumed that the 'broadband' albedo was equal to the spectral albedo of channel 1. Finally, since the first three assumptions were made without regard to surface type, the additional assumption of scene type independence was implied. This was equivalent to assuming that all surface types had similar reflectance characteristics. See Gruber, 1977 and Gruber et al., 1983 for details prior to the implementation herein described.

In spite of known deficiencies, these earlier assumptions were necessary until such time as suitable models became available. Finally, after several years of development, the requisite models did exist and, in May, 1988, were implemented in the NOAA-9 AVHRR radiation budget operation. In the following sections the currently used models and scene identification system will be described. The techniques used to implement these in the operational environment will be discussed and an attempt will be made to serially trace the events which occur as shortwave reflected data are processed. Several types of analysis will be used to compare output parameters with and without models. Finally, some description will be given of work in progress which could improve upon current results and some speculation will be made of future possibilities.

Derivation of Models

Directional and bi-directional models were derived primarily from data obtained by the Earth Radiation Budget (ERB) instrument on the Nimbus-7 satellite. More specifically, data were taken from the Nimbus-7 ERB Sub-Target Radiance Tapes (STRTs). The STRTs contain ERB radiances and associated viewing geometry which have been matched with corresponding geography and topography as well as cloud type and amount. See Stowe and Fromm, 1983, for a description of the STRTs.

The first directional and bi-directional models which were made from the STRTs were for a set of uniform earth and cloud surfaces and were described by Taylor and Stowe, 1984. More complete information describing methods used for sorting into bins, integrating, averaging, etc. may be found in that source. Many other model sets and revisions have been made since the first uniform surface set (i.e., Taylor and Stowe, 1986), but the basic techniques of model formulation are largely the same. Changes which have occurred concern the definition of surface types and calculation of cloud amounts.

A few years ago in the initial phases of the Earth Radiation Budget Experiment (ERBE), it was decided to use a set of models based upon the Nimbus-7 ERB STRT data set. The set of surface types which were chosen for ERBE (and subsequently for AVHRR processing) are listed in table 1. Though the same types are still used, many revisions of the model data have been necessary following much analysis and experimentation. One characteristic which imposes limitations on the use of Nimbus-7 ERB models is caused by the sun-synchronous nature of the Nimbus-7 orbit and its near noon daylight equatorial crossing time. Within the radiance data there is a large correlation between the solar zenith angle and latitude, so that data observed for very small solar zenith angles (near overhead) occur near the equator and data with large solar zenith angles in the polar regions. Some spread of the solar zenith angle range for any given latitude does occur because of the seasonal latitude variation of the sun (approx. 47 degrees).

The degree to which certain scene type models represent actual conditions may vary with latitude because of peculiarities with the ERB-7 data set. The availability of data for certain combinations of conditions is limited. For example, no snow data exist for small solar zenith angles since no large snow fields exist in the tropics. In other cases, data for clear land and clear ocean are very limited for large solar zenith angles since, in polar regions, these are largely obscured by sea ice, snow or cloud. The models were further modified with a variety of techniques among which were some hybridizing with characteristics of partial model sets derived from GOES satellite data. With GOES data it is possible to observe the brightness of a given scene over a complete diurnal cycle (see, for example, Minnis and Harrison, 1984). Other techniques applied were interpolation over questionable data, extrapolation into missing data, adjustment to resemble theoretical studies and even, in a few cases, appealing to what a committee of scientists felt was 'common sense' (only as a last resort). A full description of ERBE model derivation and the complete model data may be found in Suttles, et al., 1988. It is this set of ERBE directional and bi-directional models which have been implemented in the AVHRR radiation budget operation.

Scene Identification

The fundamental unit of viewed surface for which reflected radiation parameters are derived is called a 'target'. A target is the area represented by an 11 x 11 array of AVHRR GAC (Global Area Coverage) pixels. Each GAC target represents an area of approx. 45 x 45 km. effective resolution when viewed at nadir. For applications of models requiring scene identification, a single scene type is determined for an entire target and the same scene specific model parameters are applied to all 121 pixels within that target.

To begin the scene identification process, each pixel is assigned a preliminary ID. This is based upon a technique described by Ruff and Gruber, 1988, and is termed 'RuffID'. RuffID assigns to each pixel one of 36 possible types which are listed in Table 2. Each assignment depends on the attributes of the pixel (i.e., its set of channel values) as well as attributes of the entire 11 x 11 array taken as a whole.

RuffID is based upon an association of colorimetric parameters with scenes from satellite imagery whose type can be determined by a skilled analyst. The three independent parameters on which the colorimetric determination is based are spectral albedos of channels 1 and 2 and a derived channel 3 'albedo' which is determined from the measurements of channels 3 and 4. Briefly, (see Ruff and Gruber, 1988, for further details) channel 4 is used to determine a black-body temperature for the scene. Filtering the black-body energy spectrum corresponding to that temperature with the channel 3 response function yields what is presumed to be the emitted (thermal) portion of the channel 3 response. Subtracting this from the total response should leave the reflected (short-wave) portion. Dividing that by the available solar energy which has been convoluted with the channel 3 filter function produces a result which might be called the channel 3 'albedo'. Even if the term 'albedo' is not entirely appropriate, it seems that its use in this context supports an adequate determination of scene ID.

The output of RuffID is an 11 x 11 array of scene types, each numbered from 1 to 36. To determine a single target scene ID, a 36 class histogram is made from the 121 pixel IDs and the procedure depicted in the flow chart and tables on page 9 is applied. One of the 12 ERBE scene types (table 1, p.8) is assigned to the target according to the table at the bottom of page 9. After creating the histogram, it is first determined whether the population of RuffID class #5 is non-zero. That is, are any of the pixels assigned as 'desert'? If so, the absence of any cloudiness in the target is implied. For RuffID to have designated even one pixel as desert, only clear pixels of either desert or vegetated land are possible in the target. The choice of ERBE scene types is assigned to whichever type is in the majority. On the other side of the diagram, it will be seen that a test is first made for the presence of snow and/or ice. To be assigned the ERBE snow category, a majority of the target must be covered with snow and/or ice. If not, whatever snow or ice is present is then treated as if it were cloud. This seems reasonable since angular reflectance models for snow/ice most nearly resemble those for clouds and the resemblance for bi-directional models is particularly good.

To determine the overall snow or cloud cover for the target, an amount is assigned to each pixel based on the table in the middle of page 9. This amount is then converted to an interval number based on 20 intervals of 5% each. There are really 4 cloudiness intervals (clear, scattered, broken, overcast), not equally spaced. It is much faster in processing to assign IDs based upon table look-up of 20 classes than to test the limits of 4 classs. The four groups of IDs for each of the three underlying surface types are seen in the bottom table on page 9.

Table 1.

ERBE SCENE TYPES*

1. -	Clear Ocean	(0-5% cloud)		
2. -	Clear Land	(")		
3. -	Clear Desert	(")		
4. -	Clear Snow/Ice	(")		
5. -	Clear Coastal	(")		
6. -	Scattered Cloud	(5-50%)	Over	Water
7. -	" "	"	"	Land/Desert
8. -	" "	"	"	Coastal
9. -	Broken "	(50-95%)	"	Water
10. -	" "	"	"	Land/Desert
11. -	" "	"	"	Coastal
12. -	Overcast Cloud	(95-100%)		

* - as of May, 1988

Table 2.

'RuffID' Scene Types

1,2.	Clear (Snow, Ice).
3.	Overcast Cloud.
4.	Clear Vegetated Land
5.	Clear Desert (No cloud in target)
6,7,8,9.	Part Cloud over Veg.
10.	Part Cloud and Part Snow over Vegetation.
11,12,13,14.	Part Snow over Veg.
15.	Cld. and Part Cld. (No Veg., Psb. desert)
16.	Snow and Part Snow (No Veg., Psb. cloud)
17.	Clear Water.
18,19,20,21.	Part Cloud over Water.
22,23,24,25.	Part Ice over Water.
26,27,28,29.	Part (Cld+Ice) over Water.
30.	Possb. Glint with Part Cloud.
31.	Possb. Glint with Part Ice.
32.	Possb. Glint with Part (Cloud+Ice).
33.	Possb. Glint (No Cloud or Ice).
34.	Part Cloud over Coastal.
35.	Part (Snow+Ice) over Coastal.
36.	Part (Cloud+Snow+Ice) over Coastal.

When four types of mixed surfaces are given, the proportions are, 0-25%, 25-50%, 50-75%, and 75-100%, respectively.

Diagram of conversion from RuffID to ERBE ID
following creation of 36 class RuffID histogram

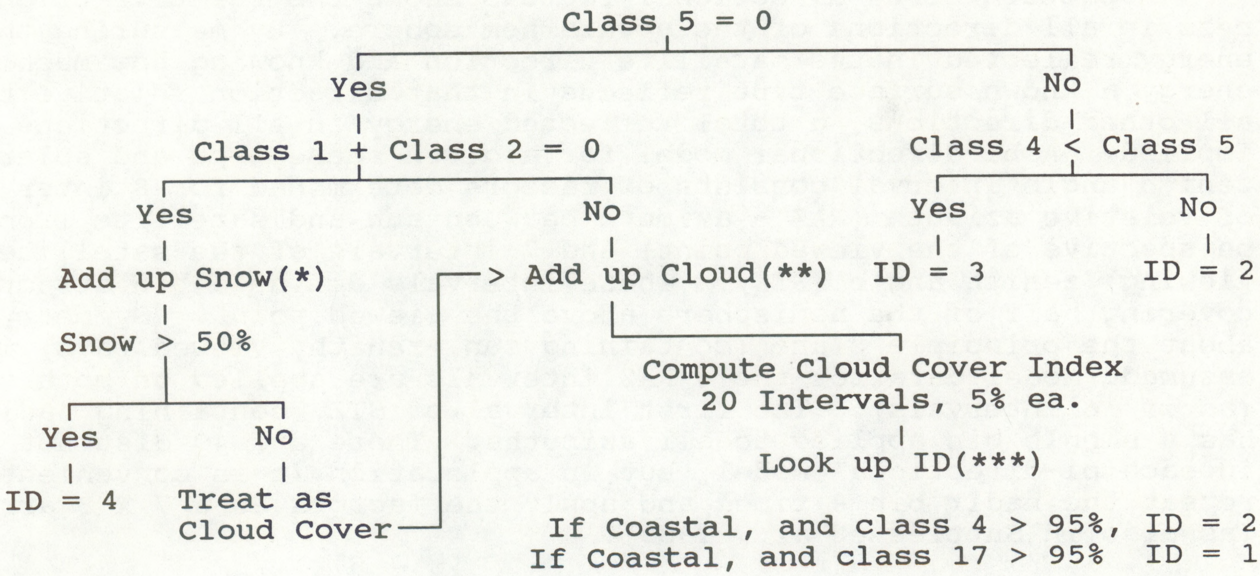

Table 3a. (*)Snow and (**)Cloud Cover for RuffID Classes

Class	Snow	Cloud	Class	Snow	Cloud	Class	Snow	Cloud
1	1.0	1.0	13	.625	.625	25	.875	.875
2	1.0	1.0	14	.875	.875	26	.0625	.125
3	0	1.0	15	0	.5	27	.1875	.375
4	0	0	16	.5	.5	28	.3125	.625
5	0	0	17	0	0	29	.4375	.875
6	0	.125	18	0	.125	30	0	.5
7	0	.375	19	0	.375	31	.5	.5
8	0	.625	20	0	.625	32	.25	.5
9	0	.875	21	0	.875	33	0	0
10	.5	.5	22	.125	.125	34	0	.5
11	.125	.5	23	.375	.375	35	.5	.5
12	.375	0	24	.625	.625	36	.25	.5

Table 3b. (***)Cloud Cover ID Lookup Table

Intvl	1	2	3	4	5	6	7	8	9	10	11	12	13	14	15	16	17	18	19	20
Land	2	7	7	7	7	7	7	7	7	7	10	10	10	10	10	10	10	10	10	12
Water	1	6	6	6	6	6	6	6	6	6	9	9	9	9	9	9	9	9	9	12
Coast	5	8	8	8	8	8	8	8	8	8	11	11	11	11	11	11	11	11	11	12

The Bi-directional Model

A pattern of bi-directional factors shows the relative brightness in all directions of the upward hemisphere. By measuring the energy reflected in the satellite direction and knowing how much energy a known surface type reflects in that direction relative to all other directions, a total reflected energy in all directions is implied. A bi-directional model for a given scene type and solar zenith angle interval consists of factors determined for 8 intervals of relative azimuth (RAZ - azimuth between sun and satellite from the perspective of the viewed point) and 7 intervals of the satellite (or viewing) zenith angle (STZ). These intervals define a bin structure covering half of the hemisphere above the viewed point. Symmetry about the principle plane (containing sun, zenith, viewed rays) is assumed. Model data for the 8 RAZ intervals are applied on both sides (as if 16 intervals). The first interval of STZ, containing nadir, has a single bin applied to all azimuths. There are 49 distinct bins in each bi-directional model, but in application it is convenient to repeat the nadir bin 8 times and apply the factors as a 7 x 8 array. (as also in Suttles et al., 1989).

The derivation of the bi-directional factors themselves begins when the source radiance data (short-wave Nimbus-7 ERB) have been sorted into the 49 bins for a particular scene type and solar zenith angle interval. An average radiance is computed for each bin and interpolation is performed when necessary to provide a value when a bin population is missing or below a certain threshold. A piece-wise constant (by bin) integration over the hemisphere is then preformed. The resultant integral is divided by pi to yield the 'equivalent isotropic radiance' and that quantity is used as a divisor for each bin average to produce the anisotropic factors.

As a sample, Fig. 1 shows analyses of anisotropic patterns for two intervals of Solar Zenith Angle (SZA). Each half of the diagram (left or right) also applies symmetrically to the other side within its own SZA interval. In polar coordinates, the radial distance represents STZ with nadir at the center and points viewed near the horizon at the outer edge. The azimuthal coordinate represents RAZ which has its origin at top center in the direction of the sun. The values of bi-directional factor shown are ratios of actual radiance to equivalent isotropic radiance. The latter quantity is a measure of the brightness the scene would have (in any direction) if the scene were isotropic and reflecting the same total energy. An anisotropic factor of 0.5 would indicate an appearance in that direction only 'half' as bright as the average, whereas a factor of 2.0 would indicate a direction in which the surface appeared 'twice' as bright.

The patterns of Fig. 1. are for clear ocean (< 5% cloud) and show quite well the effects of 'sun glint'. Note how the glint area (the maximum region near the center) moves as the sun shifts towards the horizon. The total set of bi-directional models consists of 120 such patterns (10 SZA intervals and 12 scene types).

The Directional Model

The integral described above represents the total reflected energy into the upward hemisphere. Because initially all radiance observations were normalized to overhead sun (dividing by cosine of SZA), the total reflected energy is also normalized. Dividing by available solar energy at overhead sun yields albedo. The relationship between solar zenith angle (SZA) and albedo, for a particular scene type, is known as the directional model. It is first used to normalize instantaneous reflected flux to a value at overhead sun. Secondly, the daily average flux is obtained by integrating the directional model over the daily distribution of SZAs at each site.

Fig. 2 shows selected directional models as a plot of albedo vs. SZA. This diagram shows the differences in albedos between various scene types and how these change with SZA. The directional data in this form are not actually used in the application, but are first 'normalized' to ratios of the value at an SZA of 0 degrees, or overhead sun. The models, in normalized form, are shown in figure 3. Instead of using the normalized directional models in their discrete form (the x's in fig. 3.), the data points for each individual model have been fitted (least squares) with a fifth order polynomial. The directional models are then stored for use as a 12 (scenes) by 6 (coefficients) table. It is then possible to evaluate each model continuously over the range of SZAs.

Since the directional model is a functional relationship between albedo and solar zenith angle, one must integrate that function over the actual path of the sun (or its zenith angle distribution) to obtain a daily average at each observed site. Actually carrying out the integration during the operational processing for each target retrieval would be quite time consuming. Instead, at the beginning of processing for each orbit, a numerical integration of the directional model is done at intervals over the full range of possible conditions to obtain a table of integration factors. Since the distribution of SZAs occurring during the daylight hours at any location is a function of latitude and solar declination (or time of year), the table of integration factors is evaluated at 91 latitudes (each 2 deg.), for each of the 12 scene types, and at a solar declination value occurring during the orbit. The solar declination is changing continuously, but slowly enough that assuming constancy for the period of a single orbit leads to no significant error, even at equinox time when the change is most rapid. To obtain the proper integration factor then, a column of the table just described is chosen which corresponds to the correct scene type and interpolation is made to the exact latitude. For convenience, since the daily available solar energy (a function of latitude and solar declination) is obtained by integration in much the same way as the daily average integration factor, it is evaluated and stored as a thirteenth column in the same table.

Narrow to Broadband Conversion

The formula currently used for the operational radiation budget was developed by Wydick, et al., 1987. Broadband albedo equals a linear combination of albedos from channels 1 and 2 in the proportions of .347 and .650 respectively, plus an intercept value of .00746, or equivalently, .746%. This means that channel 2 receives nearly twice the weight of channel 1 in the broadband determination. This formula resulted from a regression involving data from NOAA-7 AVHRR and Nimbus-7 ERB whose viewing conditions and scene types were matched as closely as possible. Even though regressions were done separately for a variety of scene types, the data populations within each type were quite limited. Initially, therefore, it was decided that the overall regression relationship would be more reliable.

The ERBE project has now provided comparison data between NOAA-9 AVHRR and the ERBE broadband shortwave channel in sufficient quantity to establish regression relationships for each scene type separately. When that study is completed, results will indicate whether the improvement potential will warrant implementation of a multi-scene narrow to broadband conversion algorithm.

The Operational Environment

The reflectance models were first implemented in the operational radiation budget processing of the NOAA-9 satellite during May, 1988. Since that time NOAA-11 has been launched and its AVHRR data will be processed with the same modeled system as NOAA-9. The NOAA-10 satellite has been operational during the same period, but the reflectance models have not been implemented for that system except as very limited off-line experiments. The NOAA-10 satellite has a sun-synchronous orbit (as do the other NOAA satellites), but with its 0730 local time equatorial crossing, it flies in close proximity to the day-night terminator. As a result, its AVHRR data are associated with large (near 90 deg.) solar zenith angles for which the reflectance models may be questionable because of shadowing and refraction effects.

The radiation budget processing system shares its 'front end' with the system for determining sea surface temperature. Both systems are based upon the same 11 x 11 arrays of GAC AVHRR data which are chosen to match fields-of-view of the HIRS instrument. The HIRS data are used only for target positioning and are not now used in the determination of radiation budget parameters.

The NOAA-9 satellite orbits the earth slightly more than 14 times each day. Within the daylight portion of each orbit, approx. 30000 targets are designated for the determination of radiation budget parameters. This processing load is great enough that certain shortcuts have proven necessary and these will be discussed in the following section.

Implementation Techniques

Whenever possible, program calculations are made by table lookup. That is, calculation results are pre-determined at the beginning of each orbit for all possible circumstances. Thereafter, instead of actually performing a calculation, one or more indices are determined for each independent component of the calculation and the result is taken from the table at those coordinates.

For each individual AVHRR target (11 x 11 pixels x 4 channels) it is required that all data be available. If a significant amount of GAC data were typically missing, this condition might become unnecessarily restrictive. However, it has been the case that the overwhelming majority of targets encountered are complete. The relatively few which might otherwise be recovered are not worth the time required to handle partially filled arrays. Some have expressed concern about the possible failure of channel 3, since this channel has had a tendency to be rather noisy on NOAA-9 and previous satellites. There is no alternative scene ID method currently available which does not require channel 3. The only alternative now, in the event of such a failure, would be a return to the processing system used prior to the implementation of the models herein described.

Because the directional and bi-directional models (and someday perhaps the narrow to broadband conversion) are dependent on scene ID, it is the first element to be determined, using an adaptation of the RuffID technique described above. Ultimately a scene index is calculated which designates one of the 12 ERBE scene types. A scene index applies to an entire target and the same bi-directional and directional models are applied to all pixels in each target. It might be possible to translate individual pixel scene types from RuffID into the 12 ERBE types and subsequently apply the models to pixels individually. However, at least currently, the required processing time would be prohibitive in the operational environment.

The short-wave radiation budget processing may be thought of as occurring in the following sequence of processes (in parentheses) and resultant products:

Instantaneous, narrow-band, directional reflectance ->
(narrow to broadband conversion)
-> Instantaneous, broadband, directional reflectance ->
(division by anisotropic factor)
-> Instantaneous, broadband flux ->
(multiplication by directional factor)
-> Instantaneous, normalized, broadband flux ->
(integration over daily path of sun)
-> Daily average, normalized, broadband flux.

The sequence which is, in fact, taken is somewhat different, though equivalent. The intermediate products do not exist as output data sets.

Processing Sequence

The changes made to implement the reflectance models were done almost entirely within a single sub-program named ABSORB (replacing ABSORBED) and a few other added sub-programs called by ABSORB. Intentionally, these changes were made to be transparent to the remainder of the system. All pre-existing documentation and formats remain valid.

ABSORB is called once for each AVHRR target. Within ABSORB a 'one-time' section, is executed just before the processing of the first daylight target of an orbit. This section is bypassed for all subsequent calls during that orbit. The 'one-time' section takes care of calibration lookup table construction, parameter calculations, and data input for those items which do not change during the orbit. External files which are read in at this time include solar declination and earth-sun distance factors, a table of parameters for conversion of instantaneous to daily average flux values, and the arrays containing the discrete bin values of the bi-directional models.

For all subsequent targets the first item accomplished in ABSORB is the calculation of a target relative azimuth angle (RAZ). This is done in sub-program SLNGRB using STZ, SZA and the target location, all of which are part of the input data stream. Scene identification, which follows, is done by a group of sub-programs (RUFFID, CH3AL, CHROM, TGID), and is described, in principle, above. Indices representing the solar zenith, viewing and relative azimuth angles are calculated, then used to look up the proper anisotropic factor (ANI) from the bi-directional model tables. The directional models are in ABSORB in the form of a data statement whose components are fifth order polynomial coefficients. The directional model factor (DIR) is evaluated from these. Pairs of limiting values of daily average integration factor (DIF) and available solar energy (ASE) are selected from tables read in previously and interpolation is performed to get values corresponding to the exact latitude value of the target center. An overall conversion factor (F) is obtained by the following calculation.

$$F = \frac{DIF}{ANI * DIR * ASE}$$

The single value of F derived for each target subsequently multiplies each of the 121 pixel values of broadband albedo.

Broadband albedo (BB), in percent, is obtained for each pixel, combining the calibrated measurements from channels 1 and 2 (A1, A2) according to the relatively simple 'narrow-to-broadband' model,

$$BB = .7459 + .347 * A1 + .650 * A2.$$

Daily average albedo (ALB) is obtained as an intermediate product, by ALB = F * BB, but is not stored as such. Instead, one additional calculation is made to obtain absorbed solar energy (ABS),

$$ABS = (1 - ALB) * ASE.$$

It is the 121 pixel values of ABS which are subsequently stored.

The 'retrieval' (a set of data passed to the next processing stage) for a target consists of the flux sum, the sum of squares, the 3-class histogram, counterparts of these items for outgoing long-wave (emitted) radiation, date, time, geographic location, and the angles of illumination and view of the target center. All the data for a single orbit (approx. 60000 retrievals, including both day and night data), are processed each time the retrieval system is run. The resultant retrievals are stored in a data set called the 'Initial Storage File'.

Once each day the data in the initial storage file are processed and sorted into mapped polar stereographic arrays and stored in what is known as the 'analysis' file. The analysis file contains data for the three most recent 24-hour periods. Each period contains 125 x 125 polar stereographic arrays for each combination of northern or southern hemisphere; nighttime longwave, daytime longwave or absorbed solar radiation; and the following parameters: total populations, data sums, sums of squares, and second and third class interval populations of the histograms.

Also once each day, the data in the analysis file from an appropriate 24 hour period are processed further to construct daily averages and variances for both polar stereographic and 2.5 degree latitude-longitude arrays. These, in addition to arrays of histogram interval populations, constitute the daily output of the operational radiation budget processing. A data set known appropriately as the '37-day File' contains data from the most recent set of as many days. As data from each day are added to this file, they overwrite the oldest day's data. At intervals of approximately 30 days the 37-day file is copied to tape and becomes part of a permanent archive.

Verification

Once implementation techniques are developed and prior to operational implementation, it is necessary to conduct tests to assure the absence of inadvertent errors (debugging) and to measure in some way the effect of implementation. Tests were naturally conducted at several points in the development process, first on very small data sets (individual targets and groups of targets), then with increasingly larger portions of orbits and finally on a set of three full orbits from the NOAA-7 satellite. In an 'off-line' mode, this was the practical extent of the data volume which could be processed. To go beyond this, it was necessary to implement a 'parallel' system which would run in real time as part of the operational job stream. Most of the material described here are results from these 'parallel' tests.

Figs. 4 and 5 are albedo maps from the same original data, processed without and with models, respectively. They are shown to demonstrate that the reflected data have not been 'scrambled' by use of the models. That is, the same organization of data (land, ocean, cloud systems etc.) in fig. 4, without models, is also present in fig. 5, where models were applied. The maps are sectors of contoured analyses from daily, 2.5 deg. latitude/longitude arrays of albedo. The albedo data are calculated from similarly configured arrays of absorbed solar radiation. Each map shown is from an array which is dimensioned as 51 latitude points by 37 longitude points and covers approximately one forth of the world between 62.5 deg. north and south.

In overall appearance, comparing fig. 4 with fig. 5, it seems that the models had a rather small effect and systematic differences are hard to detect. When examining differences between modeled and unmodeled, however, as in Figure 6.(solid-positive, dashed-negative), changes are much more apparent and appear to be organized into elongated features paralleling the orbital tracks. Such a difference pattern was expected, if the models had their desired effect. It has long been known that uncorrected reflectance data are affected by the relative conditions of illumination and view. For a sun synchronous polar orbiting satellite, these conditions are repeated from one orbit to the next. Nowhere are these effects more obvious than in a photographic global montage of several orbits. In such a display the western side of an orbit would usually be systematically lighter or darker than the eastern side. The darker side of one orbit then abuts the lighter side of the adjacent orbit causing an abrupt change which has nothing to do with changing surface type.

Even if such a difference pattern as seen in fig. 6 is expected, these figures (4,5,6) do not show if the magnitude of the effect is correct. Could the models have taken out too little of the undesirable pattern, or have introduced the same pattern with the opposite sign by making too large of a correction? That such is not the case may be seen in fig. 7. The auto-correlation functions which are shown are constructed from arrays such as those analyzed in figs. 4 and 5, but using instead the entire 2.5 deg. global latitude/longitude array between 62.5 deg. north and south. Each cylindrical array has dimensions of 51 latitude points by 144 longitude points. The left and right edges are considered to be adjacent columns. The correlation function is calculated between two identical arrays (i.e. correlating an array with itself). This is done by calculating the correlation coefficient between them and then, in a series of steps, shifting one of them by 2.5 deg. of longitude and recalculating. The arrays start in perfect correlation and 144 shifts are can be made before they return to that state. The direction of shift does not matter since the two halves of each correlation coefficient set are symmetric. Only half, therefore, of each total function has been plotted. The repeating pattern is clearly seen in the uncorrected data. The relative smoothness of the other curve demonstrates that this pattern has been largely removed by the implementation of the models. The patterns of viewing and illumination angles repeat almost exactly from orbit to orbit for a sun-synchronous satellite and except for the modulating effects of variable cloudiness and changes in underlying scene type, the amplitude of the correlation would probably return to near 100% in each oscillation.

The same result demonstrated by fig. 7 can be illustrated in a different way by doing a spectrum analysis of the auto-correlation functions. The two spectra are plotted in fig. 8. The 'spike' in the uncorrected data, has only a small residual in the corrected spectrum, and occurs at a frequency corresponding to the number of orbits which occur in one day (or 360 deg. of longitude).

Effects of overlapping coverage occur in the mapped arrays increasingly toward the poles. Whereas data from the tropics and mid-latitudes generally are from single orbits, data from polar regions are averages of multiple views from two to several orbits. This averaging process tends to obscure some of the effects described above caused by longitudinal repeating patterns of viewing and illumination conditions. Note that the cross-track scan of the NOAA satellites is more in the direction of changing latitude in the polar regions and in the direction of changing longitude in tropical regions. To illustrate some model effects in the polar regions, another type of display will be used which will compare individual grid points.

Fig. 9 shows daily time series of albedo, with and without models, calculated for the grid point centered on the South Pole. Fig. 10 shows a similar display for another point on the Antarctic continent which is 15 deg. of latitude from the pole. Certainly both areas are permanently snow covered and it is reasonable to think they would have similar albedos, though not necessarily equal. By examining the satellite scan pattern near the pole, and deducing the viewing geometry involved, it can be verified that the anisotropic factors of the two points are quite different. In one case the anisotropic factor is less than one, and that correction is upward (the factor is used as a divisor). In the other case, the factor is greater than one and the correction downward. Indeed, in these diagrams it is seen that the models systematically lowered the albedo of the pole from 75-80% to about 70% while raising the albedo of the other snow point from about 60% to about 75%. Lacking 'ground truth' data, it is not possible to say how nearly correct either point's modeled albedos are in an absolute sense. However, the albedos for similar surfaces becoming more nearly equal on the one hand and both becoming nearer to the global average albedo for snow (see fig. 2) on the other are promising, if not conclusive, indications.

Figures 11 - 14 comprise a set similar to figs. 9 - 10, but these locations have latitudes within boundaries mentioned in the description of fig. 7. They were chosen somewhat randomly to contain a wide variety of surface and weather types. Whereas the two polar points described above showed uncorrected (or model effect) biases in opposite directions, this set of points shows little overall bias one way or the other. They all, however, show an oscillating bias which is probably the effect of oscillating viewing angles as the data are seen in different parts of the orbit on succeeding days.

Conclusions and Prospects for Change

It has been reasonably well demonstrated that the implementation of reflectance models represents a significant improvement in the retrieval of short-wave radiation budget parameters from AVHRR. Clearly, some negative features known to be associated with the previous version have been removed. It is, however, difficult to judge how 'good' the product really is. This is because no good 'ground truth' data exist with which to make a comparison. The best that can be done in this regard is probably to do comparisons with results from the ERBE experiment.

Shortcuts have admittedly been taken in the model implementation, such as the application of models to targets rather than to individual pixels and a conversion method to estimate broadband radiance from narrow band which is based on a too small statistical sample. The first of these is required by the operational environment and is not likely to change in the foreseeable future. The second, on the other hand, should be significantly improved as co-located AVHRR and ERBE data are analyzed. Other improvements will await results of ERBE investigations as well as our own studies which will deal specifically with the AVHRR product. In regard to the latter consideration, we look forward to developing a processing system which will allow research of AVHRR radiation budget processing in a true off-line mode which will neither affect, nor be affected by, the on-going operation. Currently, tests must be run as part of the operational job stream, thereby competing with other operational tasks for computer resources and the attention of available operations personnel. In this, the tests receive a rather low priority.

The scene ID may be modified in order to have it identify cloud amounts which will correspond in their totals to generally accepted amounts for global cloudiness. This can easily be done by adjusting arbitrary factors in the program. Several other AVHRR cloud retrieval algorithms are under development at NESDIS which may eventually prove to be superior to the method currently in use. Comparisons between these methods will be very useful. The effect on radiation parameters of changing the scene ID will certainly be one of the subjects of 'off-line' testing mentioned above.

References

1. Gruber, A., 1977: Determination of the Earth-atmosphere Radiation Budget from NOAA Satellite Data. NOAA Technical Report NESS 76, U. S. Dept. Comm., NOAA, NESS, Washington D. C. 28p.

2. Gruber, A., I. S. Ruff and C. Earnest, 1983: Determination of the Planetary Radiation Budget from TIROS-N Satellites. NOAA Technical Report NESDIS 3, U. S. Dept. Comm., NOAA, NESDIS, Washington D. C. 12p.

3. Minnis, P. and E. F. Harrison, 1984: Diurnal Variability of Regional Cloud and Clear-sky Radiative Parameters Derived from GOES Data. Part III: November 1978 Radiative Parameters. J. Clim. & Appl. Meteorol., vol.23, no.7, July, pp.1032-1051.

4. Ruff, I. S. and A. Gruber, 1988: General Determination of Earth Surface Type and Cloud Amount Using Multispectral AVHRR Data, NOAA Technical Report NESDIS 39, U. S. Dept. Comm., NOAA, NESDIS, Washington D. C. 30 p.

5. Stowe L. L. and M. D. Fromm, 1983: Nimbus-7 ERB Sub-Target Radiance Tape (STRT) Data Base. NOAA Tech. Memo. NESDIS 3, U. S. Dept. Comm., NOAA, NESDIS, Washington D. C. 71 p.

6. Suttles, J. T., R. N. Green, P. Minnis, G. L. Smith, W. F. Staylor B. A. Wielicki, I. J. Walker, D. F. Young, V. R. Taylor and L. L. Stowe, 1988: Angular Radiation Models for Earth-Atmosphere System. Vol. 1 - Shortwave Radiation. NASA Reference Publication 1184, NASA-Langley, Hampton, VA 144p.

7. Taylor, V. R. and L. L. Stowe, 1984: Reflectance Characteristics of Uniform Earth and Cloud Surfaces Derived from Nimbus-7 ERB, J. Geophys. Res., Vol.89, no.D4, June 30, pp. 4987-4996.

8. Taylor, V. R. and L. L. Stowe, 1986: Revised Reflectance and Emission Models From Nimbus-7 ERB Data. Sixth Conference on Atmospheric Radiation, Williamsburg, VA, American Meteorological Soc., pp. J19-J22.

9. Wydick, J. E., P. A. Davis and A. Gruber, 1987: Estimation of Broadband Planetary Albedo from Operational Narrowband Satellite Measurements, NOAA Technical Report NESDIS 27, U. S. Dept. Comm., NOAA, Washington D. C., May.

NIMBUS-7 ERB BI-DIRECTIONAL REFLECTANCE

SUN

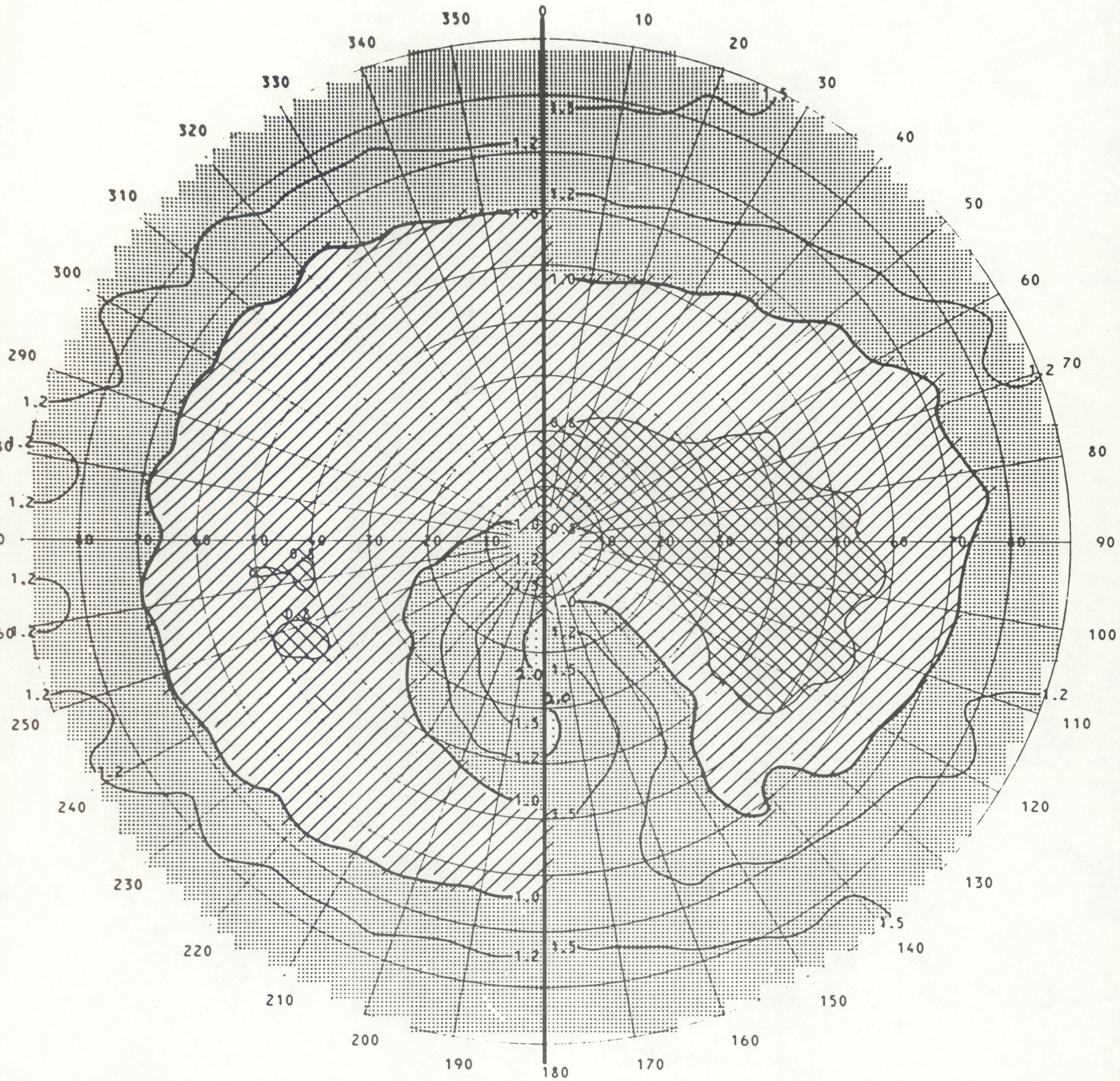

ALBEDO=.08
POPULATION= 87010
SO!AR ZENITH ANG (0.0-25.8)
INTEGRAL= 106.8 INTEGRA'/PI= 34.0

ALBEDO=.08
POPULATION= 45205
SOLAR ZENITH ANG (25.8-36.9)
INTEGRAL= 115.2 INTEGRAL/PI= 36.6

CLEAR OCEAN

Fig. 1

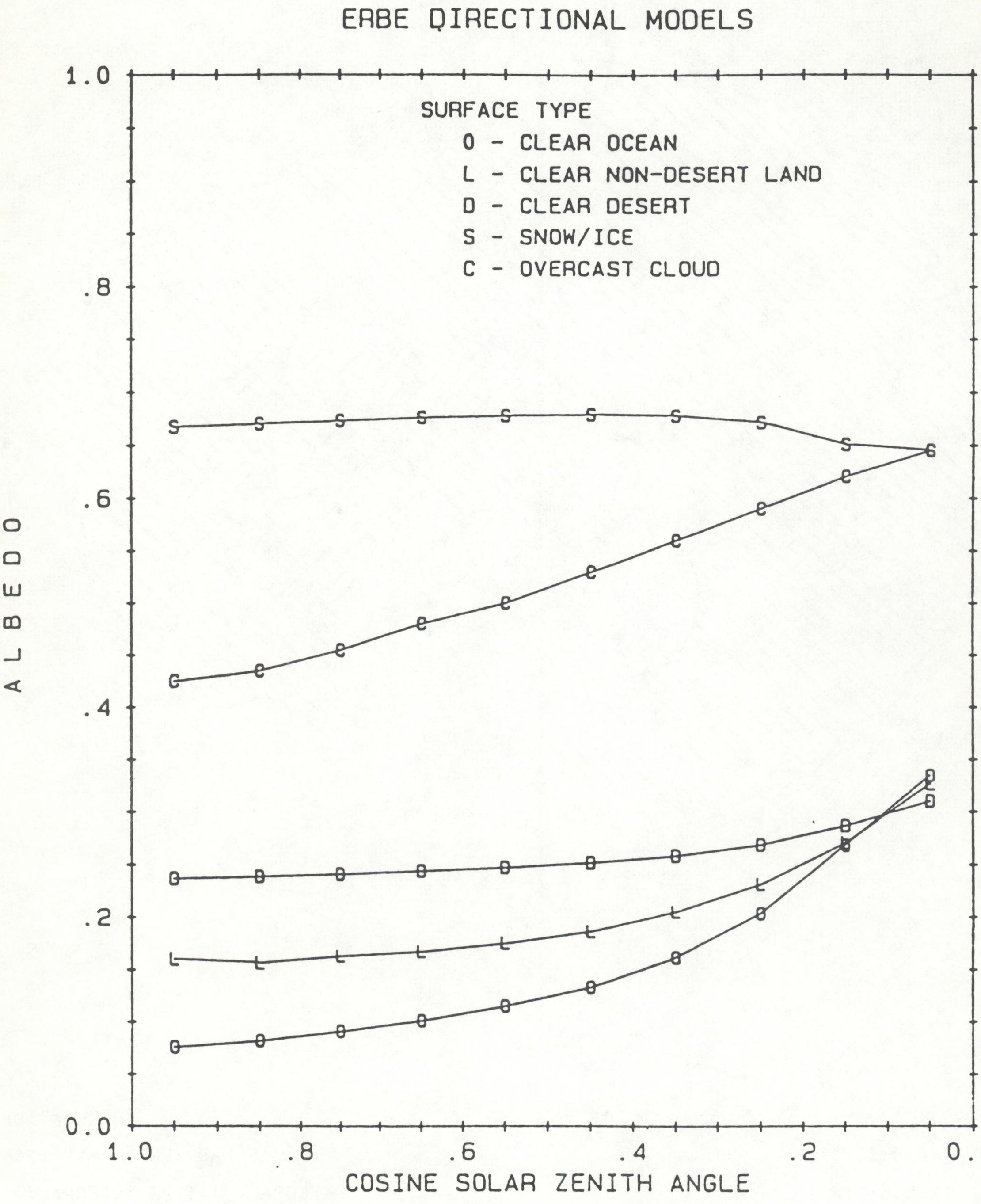

ERBE DIRECTIONAL MODELS
SURFACE TYPE
O - CLEAR OCEAN
L - CLEAR NON-DESERT LAND
D - CLEAR DESERT
S - SNOW/ICE
C - OVERCAST CLOUD
ALBEDO
COSINE SOLAR ZENITH ANGLE
1.0
.8
.6
.4
.2
0.0

Fig. 2

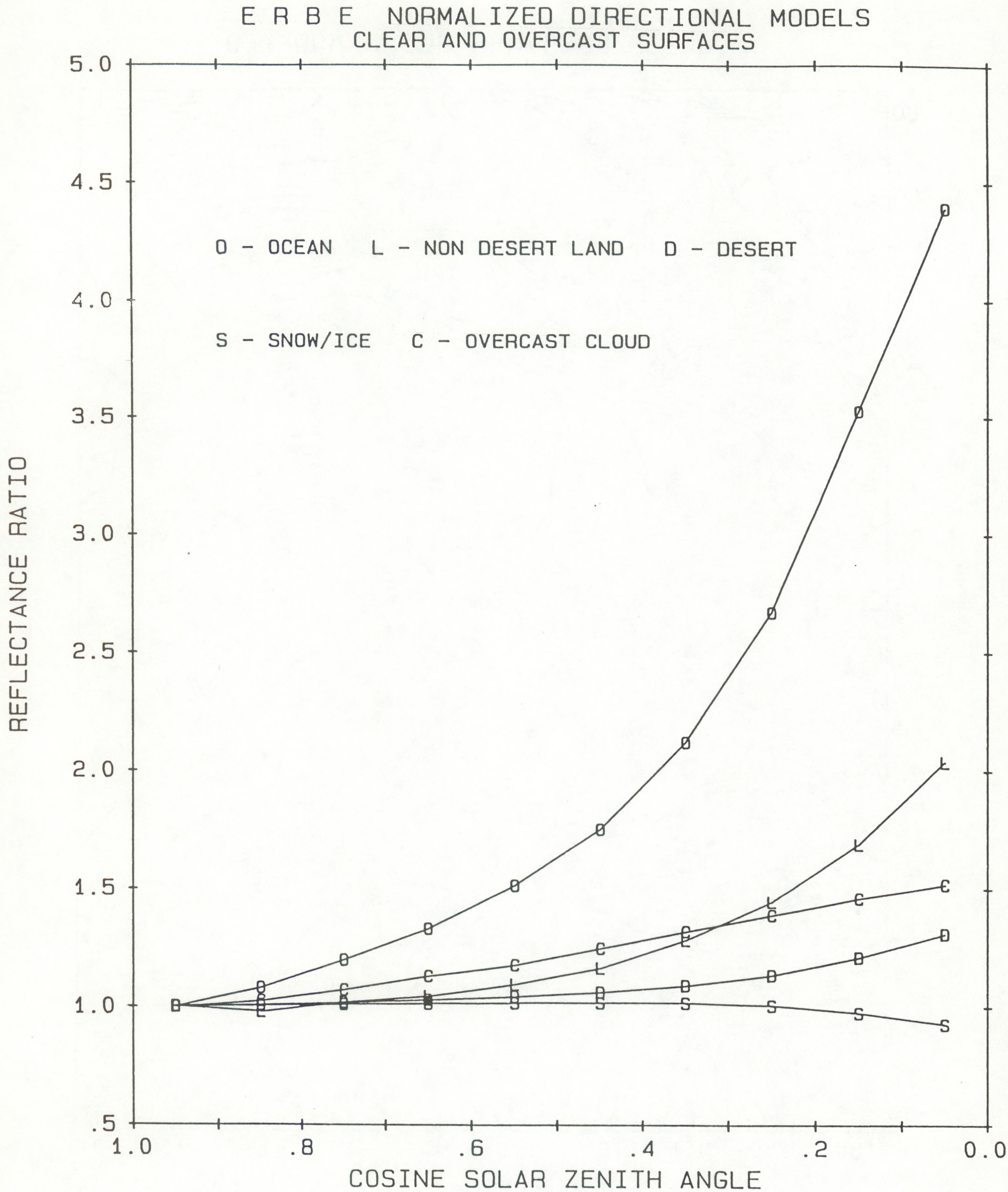
E R B E NORMALIZED DIRECTIONAL MODELS
CLEAR AND OVERCAST SURFACES
O - OCEAN L - NON DESERT LAND D - DESERT
S - SNOW/ICE C - OVERCAST CLOUD
REFLECTANCE RATIO
COSINE SOLAR ZENITH ANGLE
5.0
4.5
4.0
3.5
3.0
2.5
2.0
1.5
1.0
.5
1.0
.8
.6
.4
.2
0.0

Fig. 3

04/18/88 AVHRR ALB UNMODELED

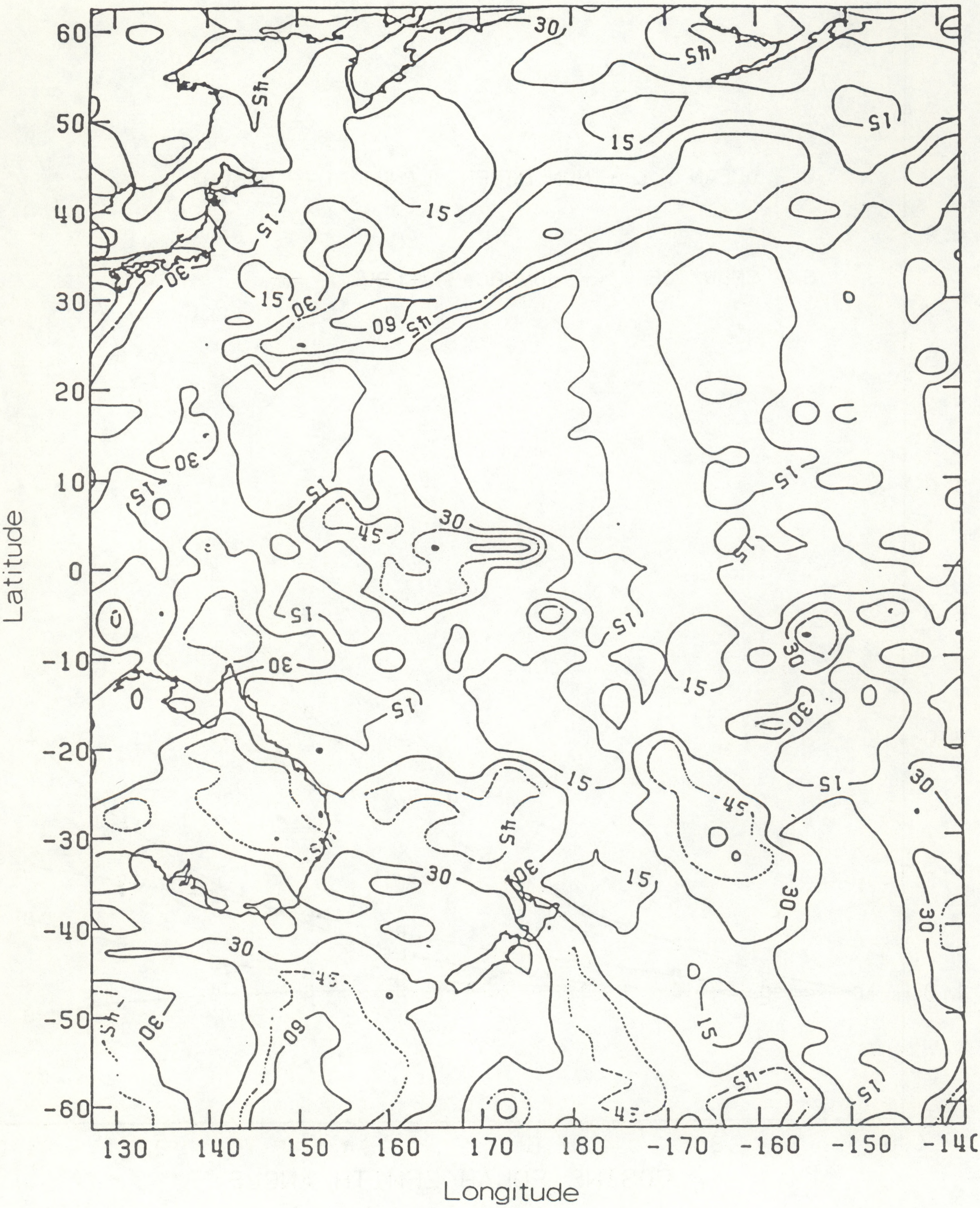

Fig. 4

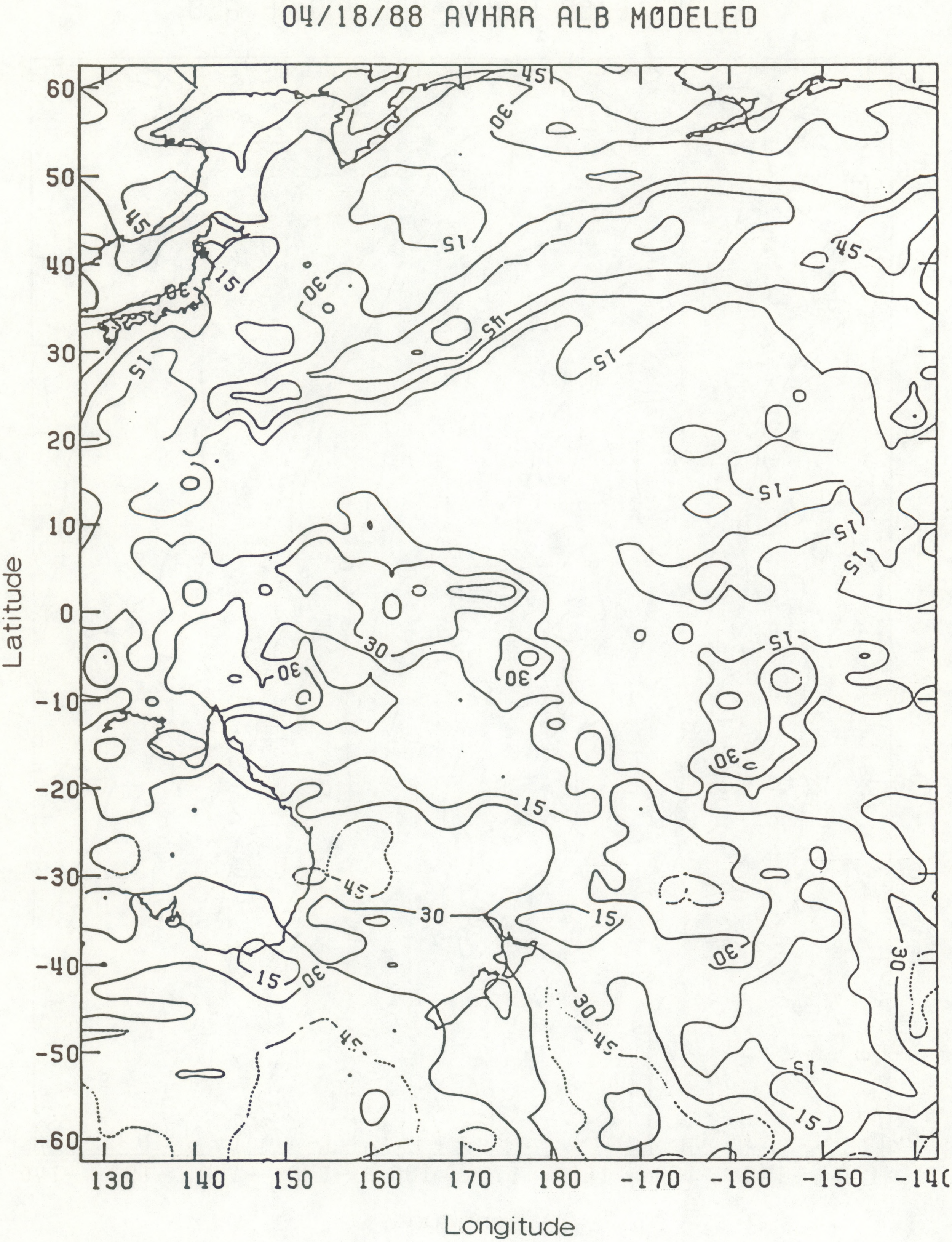

04/18/88 AVHRR ALB MØDELED
Latitude
Longitude
60
50
40
30
20
10
0
-10
-20
-30
-40
-50
-60
130
140
150
160
170
180
-170
-160
-150
-140
15
30
45

Fig. 5

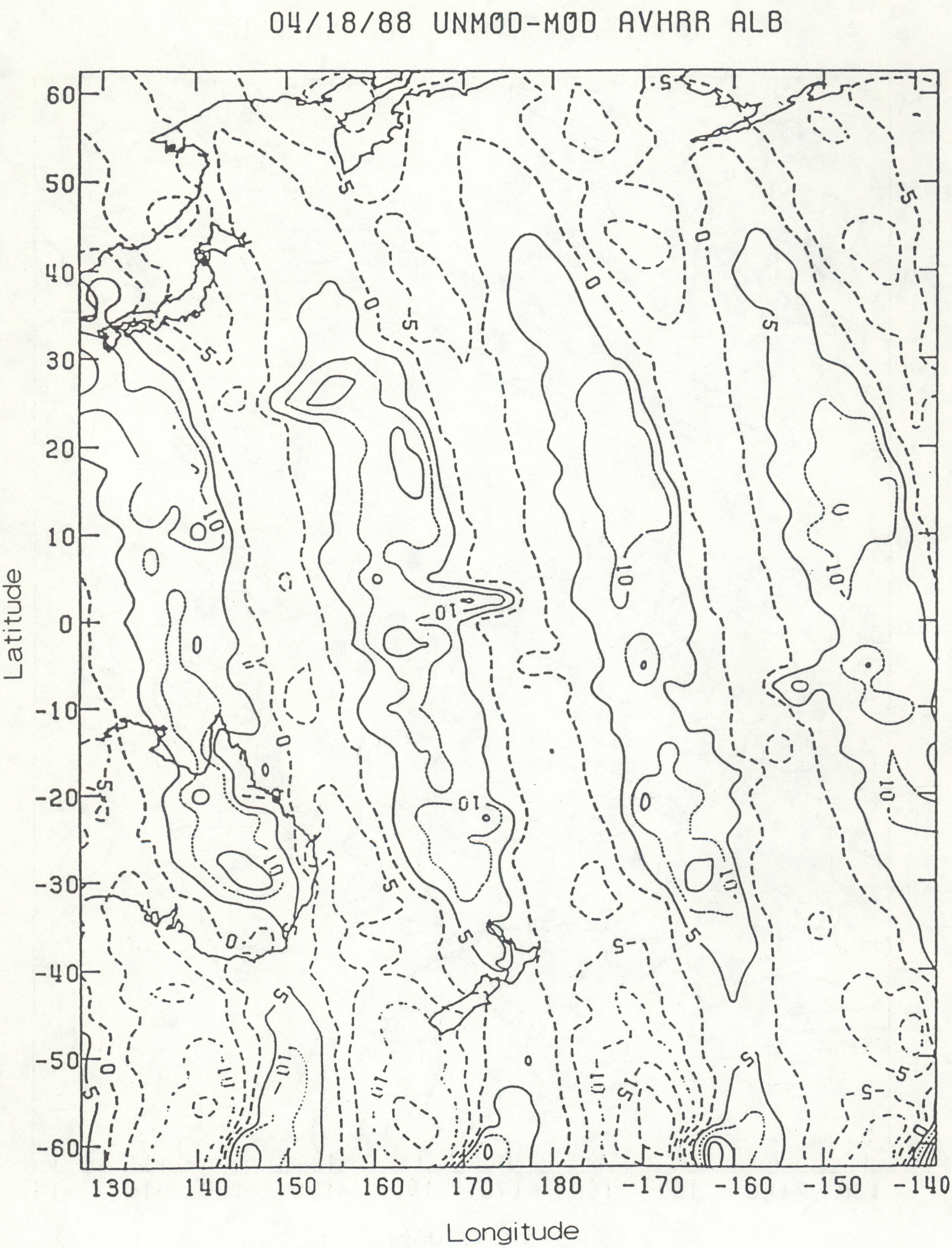
04/18/88 UNMOD-MOD AVHRR ALB
60
50
40
30
20
10
0
-10
-20
-30
-40
-50
-60
Latitude
130
140
150
160
170
180
-170
-160
-150
-140
Longitude

Fig. 6

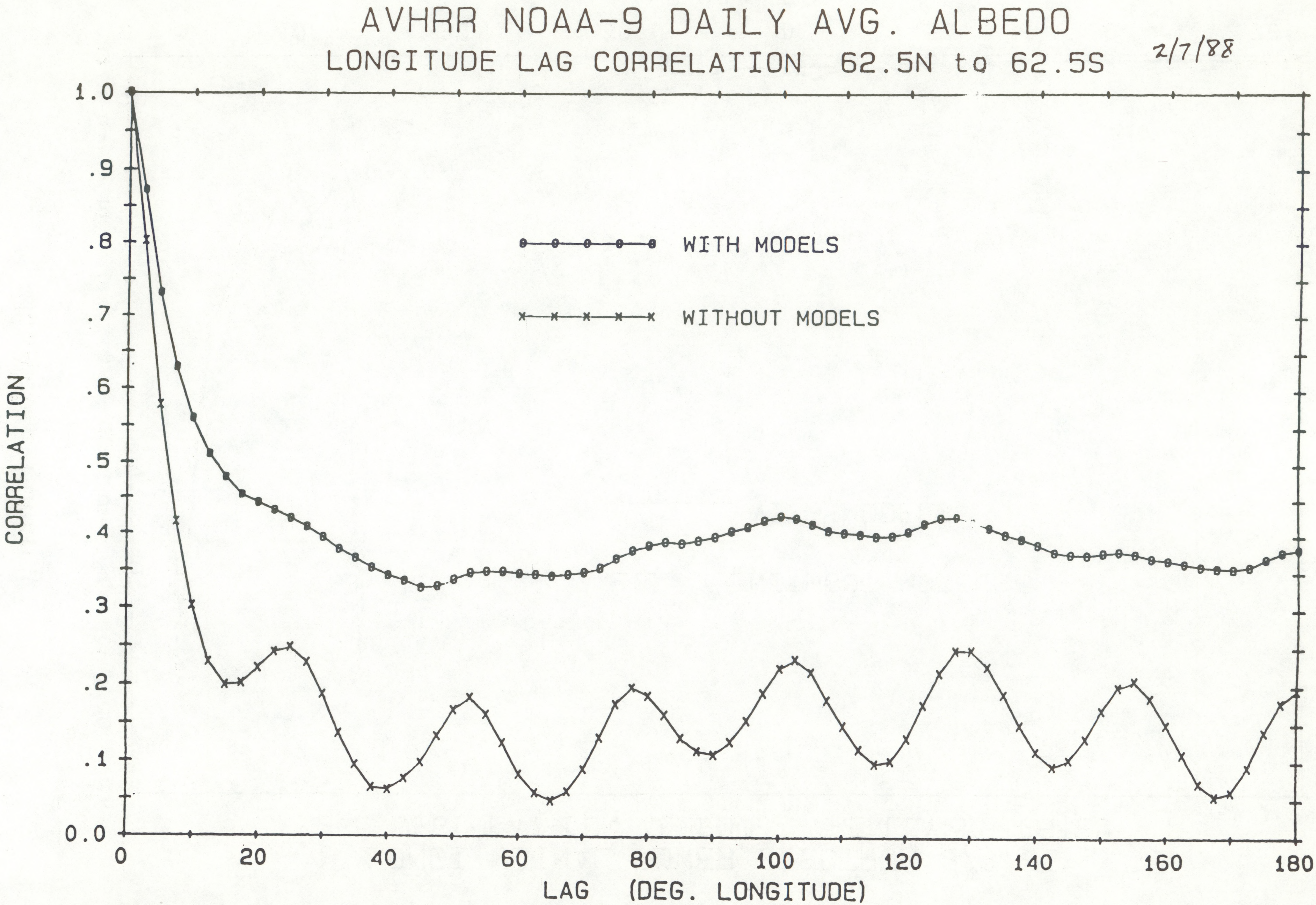
AVHRR NOAA-9 DAILY AVG. ALBEDO
LONGITUDE LAG CORRELATION 62.5N to 62.5S
2/7/88
WITH MODELS
WITHOUT MODELS
CORRELATION
1.0
.9
.8
.7
.6
.5
.4
.3
.2
.1
0.0
0
20
40
60
80
100
120
140
160
180
LAG (DEG. LONGITUDE)

Fig. 7

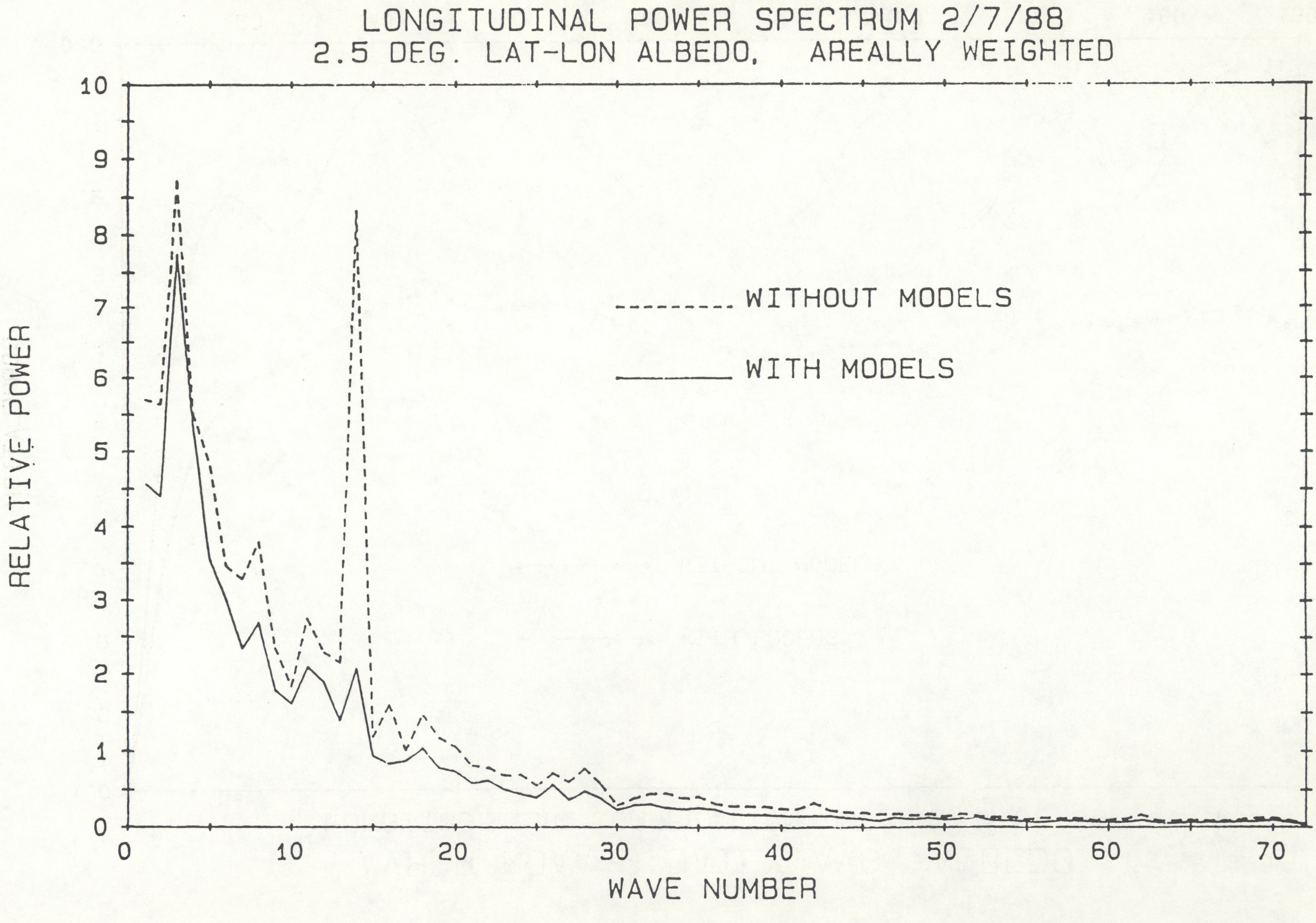
LONGITUDINAL POWER SPECTRUM 2/7/88
2.5 DEG. LAT-LON ALBEDO, AREALLY WEIGHTED
WITHOUT MODELS
WITH MODELS
RELATIVE POWER
WAVE NUMBER
0
1
2
3
4
5
6
7
8
9
10
20
30
40
50
60
70

Fig. 8

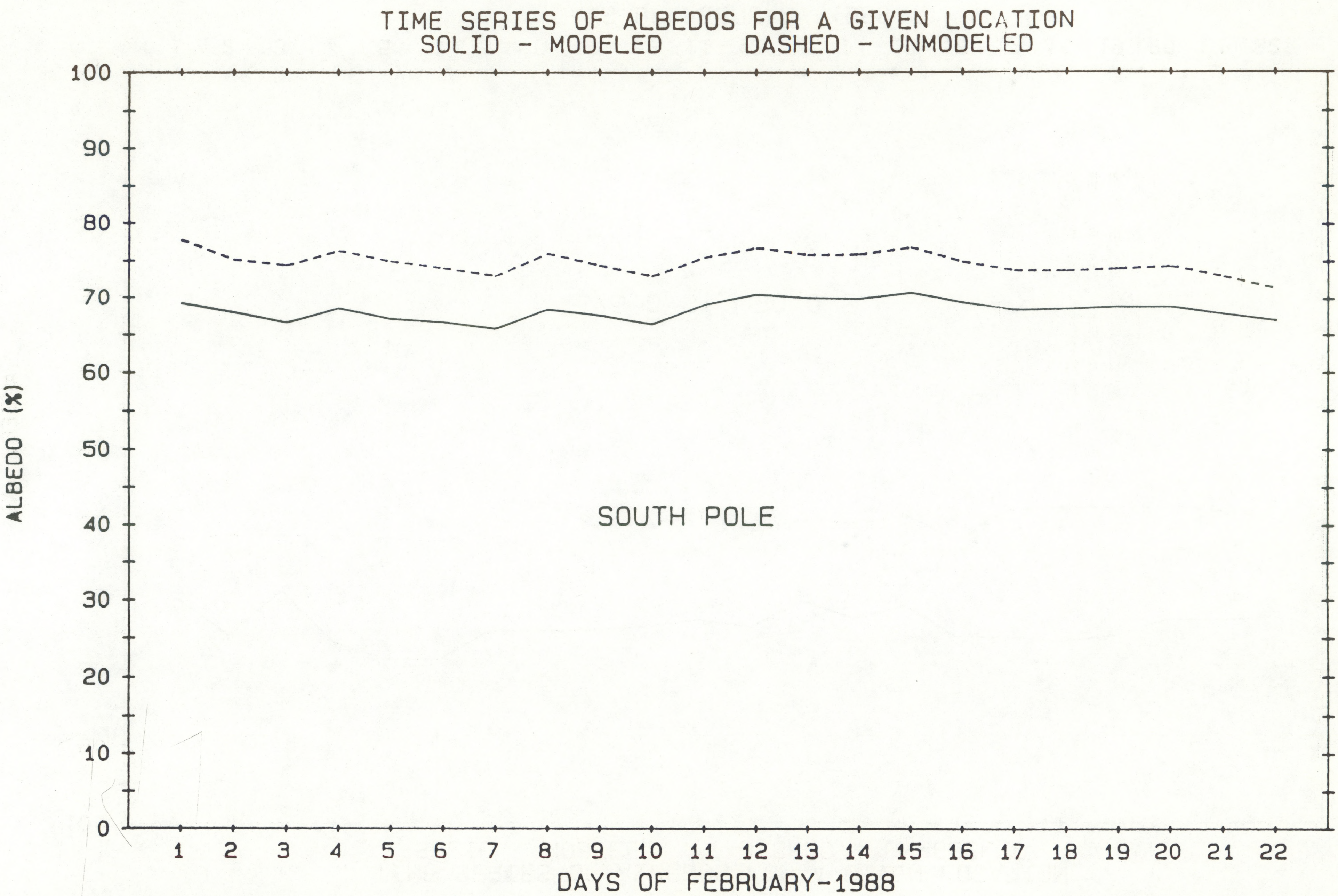
TIME SERIES OF ALBEDOS FOR A GIVEN LOCATION
SOLID - MODELED DASHED - UNMODELED
ALBEDO (%)
0
10
20
30
40
50
60
70
80
90
100
SOUTH POLE
1 2 3 4 5 6 7 8 9 10 11 12 13 14 15 16 17 18 19 20 21 22
DAYS OF FEBRUARY-1988

Fig. 9

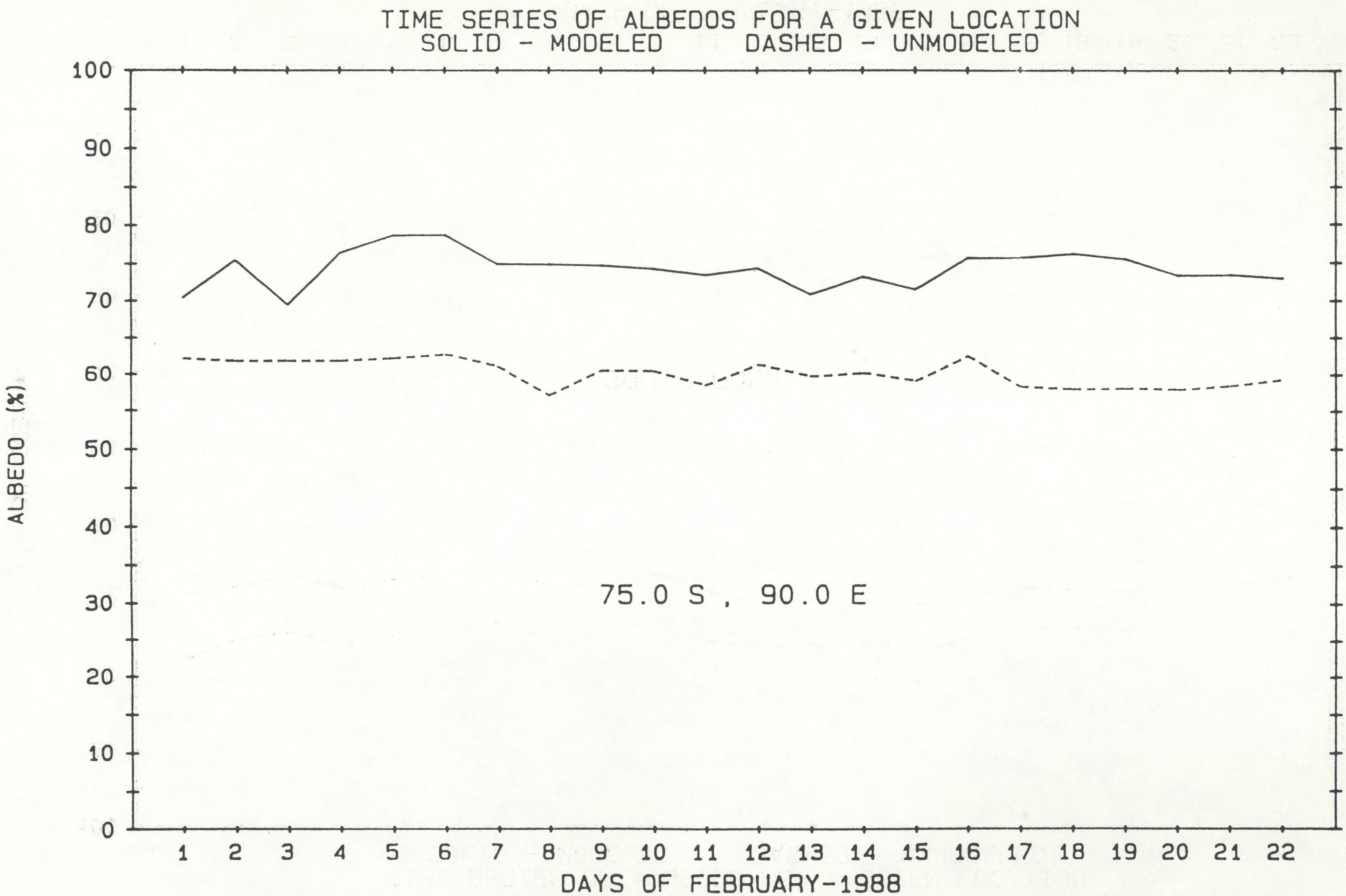
TIME SERIES OF ALBEDOS FOR A GIVEN LOCATION
SOLID - MODELED DASHED - UNMODELED
100
90
80
70
60
50
40
30
20
10
0
ALBEDO (%)
75.0 S , 90.0 E
1 2 3 4 5 6 7 8 9 10 11 12 13 14 15 16 17 18 19 20 21 22
DAYS OF FEBRUARY-1988

Fig. 10

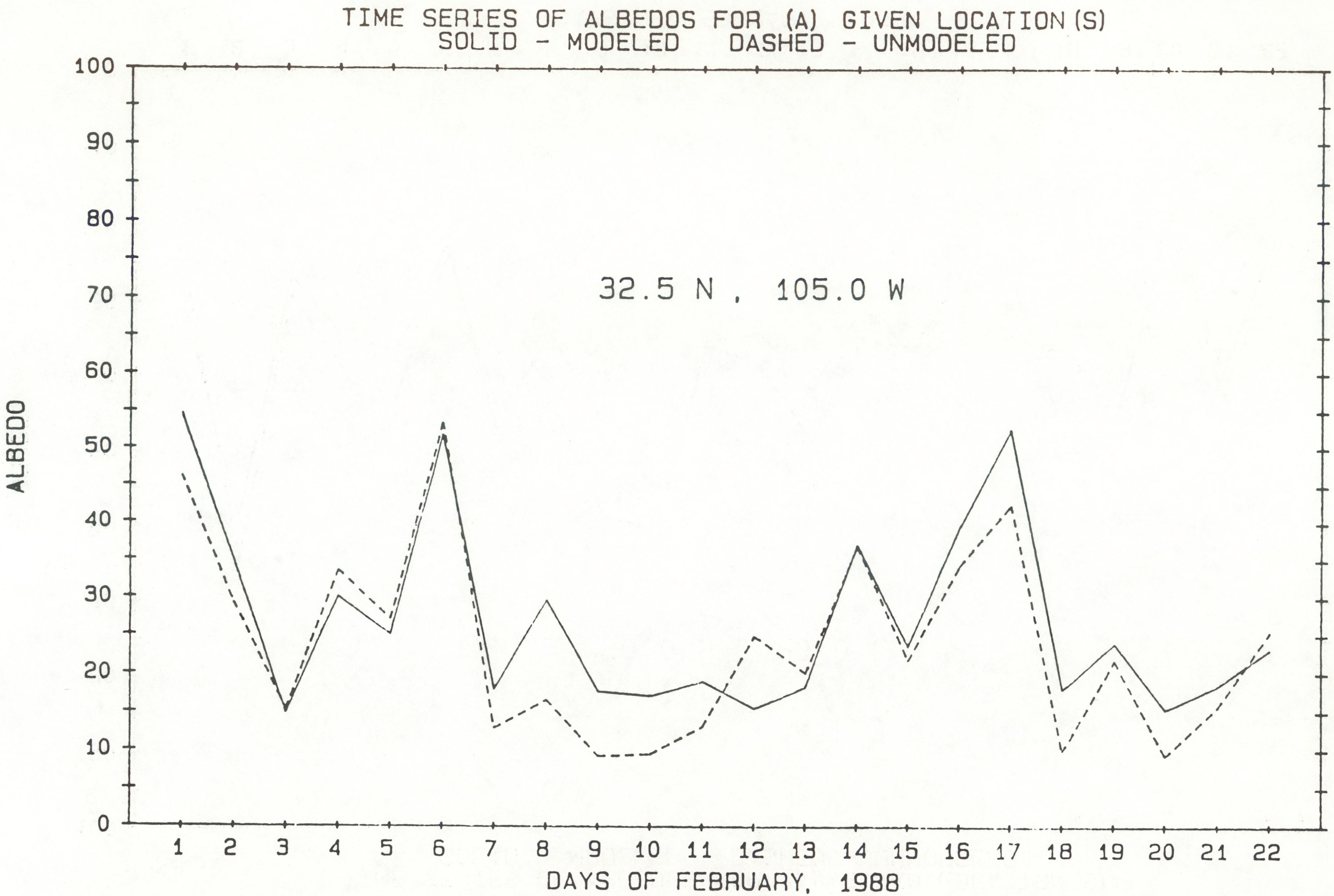
TIME SERIES OF ALBEDOS FOR (A) GIVEN LOCATION (S)
SOLID - MODELED DASHED - UNMODELED
32.5 N , 105.0 W
ALBEDO
0
10
20
30
40
50
60
70
80
90
100
1 2 3 4 5 6 7 8 9 10 11 12 13 14 15 16 17 18 19 20 21 22
DAYS OF FEBRUARY, 1988

Fig. 11

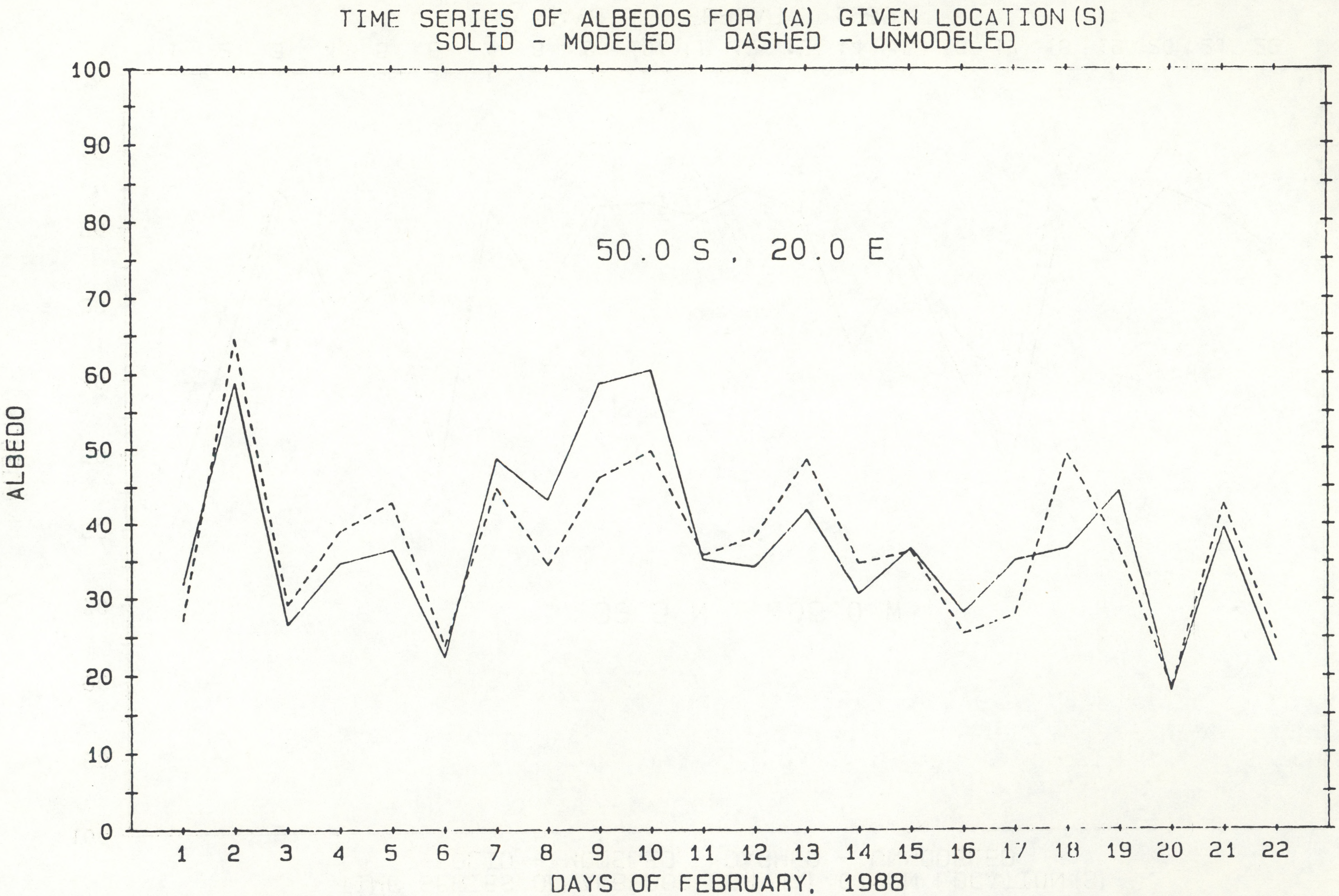
TIME SERIES OF ALBEDOS FOR (A) GIVEN LOCATION (S)
SOLID - MODELED DASHED - UNMODELED
50.0 S , 20.0 E
ALBEDO
0
10
20
30
40
50
60
70
80
90
100
1 2 3 4 5 6 7 8 9 10 11 12 13 14 15 16 17 18 19 20 21 22
DAYS OF FEBRUARY, 1988

Fig. 12

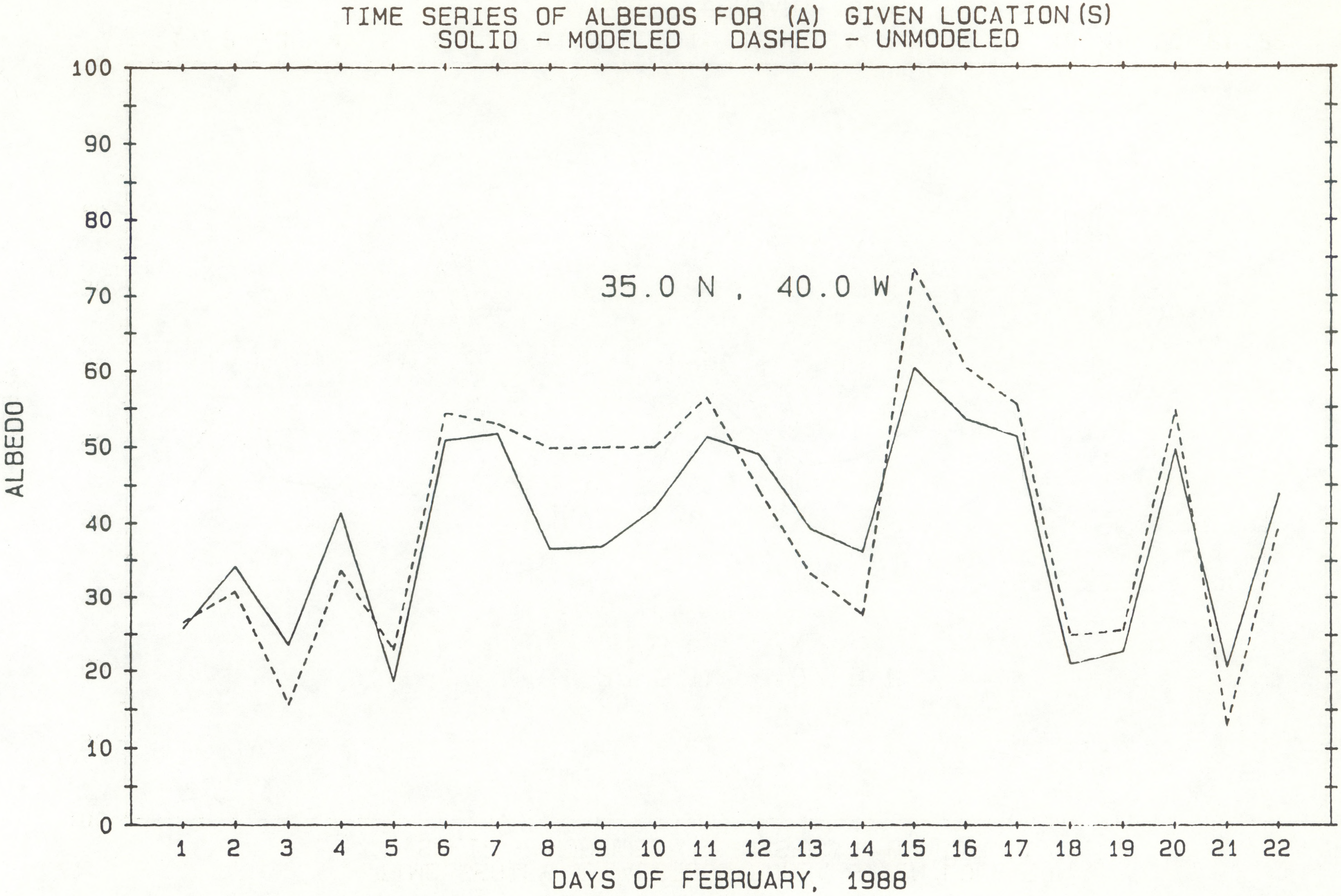
TIME SERIES OF ALBEDOS FOR (A) GIVEN LOCATION (S)
SOLID - MODELED DASHED - UNMODELED
35.0 N , 40.0 W
ALBEDO
100
90
80
70
60
50
40
30
20
10
0
1 2 3 4 5 6 7 8 9 10 11 12 13 14 15 16 17 18 19 20 21 22
DAYS OF FEBRUARY, 1988

Fig. 13

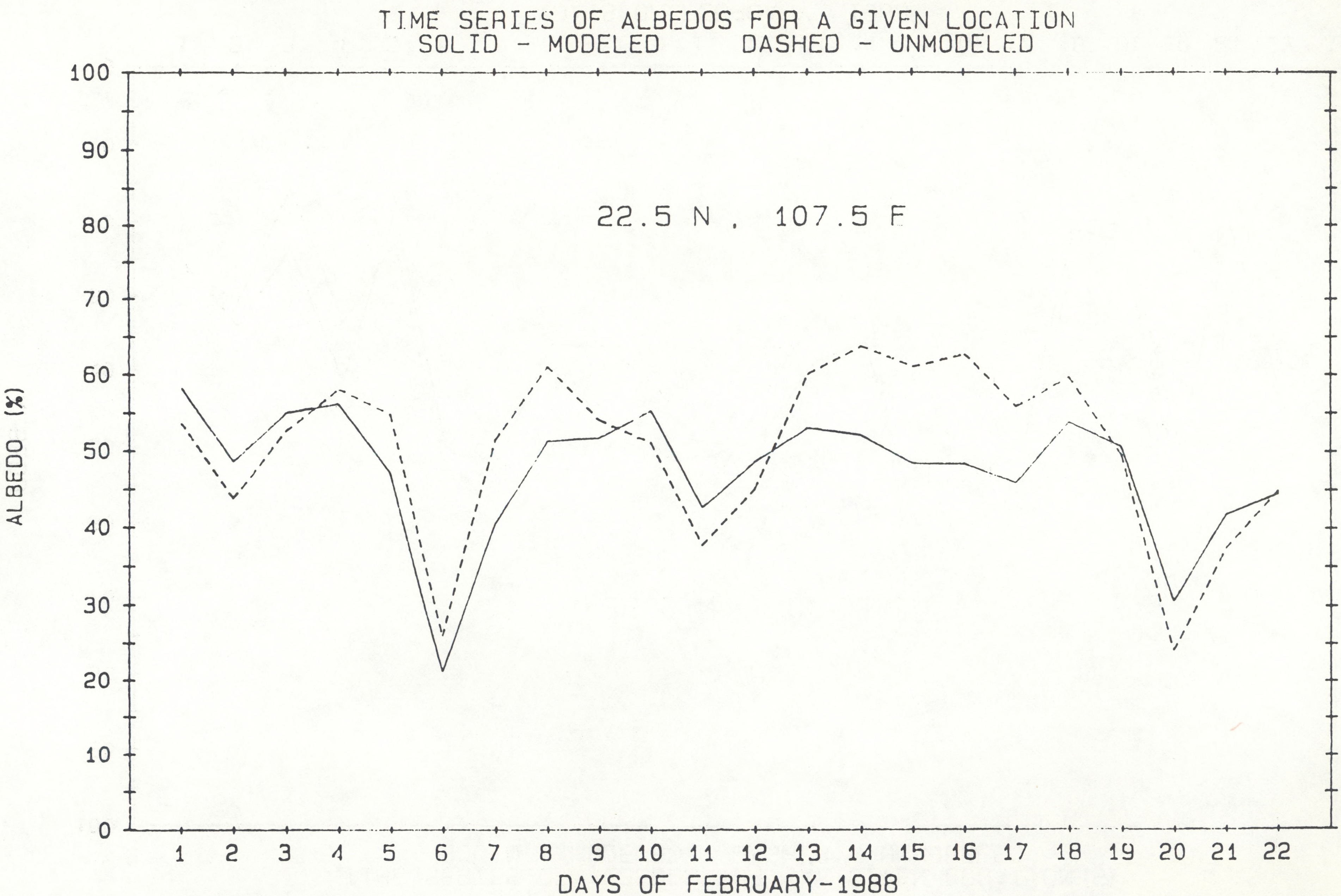
TIME SERIES OF ALBEDOS FOR A GIVEN LOCATION
SOLID - MODELED DASHED - UNMODELED
22.5 N , 107.5 E
ALBEDO (%)
100
90
80
70
60
50
40
30
20
10
0
1 2 3 4 5 6 7 8 9 10 11 12 13 14 15 16 17 18 19 20 21 22
DAYS OF FEBRUARY-1988

Fig. 14

(Continued from inside front cover)

NESDIS 18 Earth Observations and the Polar Platform. John H. McElroy and Stanley R. Schneider, January 1985. (PB85 177624/AS)

NESDIS 19 The Space Station Polar Platform: Intergrating Research and Operational Missions. John H. McElroy and Stanley R. Schneider, January 1985. (PB85 195279/AS)

NESDIS 20 An Atlas of High Altitude Aircraft Measured Radiance of White Sands, New Mexico, in the 450-1050nm Band. Gilbert R. Smith, Robert H. Levin and John S. Knoll, April 1985. (PB85 204501/AS)

NESDIS 21 High Altitude Measured Radiance of White Sands, New Mexico, in the 400-2000nm Band Using a Filter Wedge Spectrometer. Gilbert R. Smith and Robert H. Levin, April 1985. (PB85 206084/AS)

NESDIS 22 The Space Station Polar Platform: NOAA Systems Considerations and Requirements. John H. McElroy and Stanley R. Schneider, June 1985. (PB86 6109246/AS)

NESDIS 23 The Use of TOMS Data in Evaluating and Improving the Total Ozone from TOVS Measurements. James H. Lienesch and Prabhat K.K. Pandey, July 1985. (PB86 108412/AS)

NESDIS 24 Satellite-Derived Moisture Profiles. Andrew Timchalk, April 1986. (PB86 232923/AS)

NESDIS 25 reserved

NESDIS 26 Monthly and Seasonal Mean Outgoing Longwave Radiation and Anomalies. Arnold Gruber, Marylin Varnadore, Phillip A. Arkin, and Jay S. Winston, October 1987. (PB87160545/AS)

NESDIS 27 Estimation of Broadband Planetary Albedo from Operational Narrowband Satellite Measurements. James Wydick, April 1987. (PB88-107644/AS)

NESDIS 28 The AVHRR/HIRS Operational Method for Satellite Based Sea Surface Temperature Determination. Charles Walton, March 1987. (PB88-107594/AS)

NESDIS 29 The Complementary Roles of Microwave and Infrared Instruments in Atmospheric Sounding. Larry McMillin, February 1987. (PB87 184917/AS)

NESDIS 30 Planning for Future Generational Sensors and Other Priorities. James C. Fischer, June 1987. (PB87 220802/AS)

NESDIS 31 Data Processing Algorithms for Inferring Stratospheric Gas Concentrations from Balloon-Based Solar Occultation Data. I-Lok Chang (American University) and Michael P. Weinreb, April 1987. (PB87 196424)

NESDIS 32 Precipitation Detection with Satellite Microwave Data. Yang Chenggang and Andrew Timchalk, June 1988. (PB88-240239)

NESDIS 33 An Introduction to the GOES I-M Imager and Sounder Instruments and the GVAR Retransmission Format. Raymond J. Komajda (Mitre Corp) and Keith McKenzie, October 1987. (PB88-132709)

NESDIS 34 Balloon-Based Infrared Solar Occultation Measurements of Stratospheric O3, H2O, HNo3, and CF2Cl2. Michael P. Weinreb and I-Lok Chang (American University), September 1987. (PB88-132725)

NESDIS 35 Passive Microwave Observing From Environmental Satellites, A Status Report Based on NOAA's June 1-4, 1987, Conference in Williamsburg, Virginia. James C. Fischer, November 1987. (PB88-208236)

NESDIS 36 Pre-Launch Calibration of Channels 1 and 2 of the Advanced Very High Resolution Radiometer. C.R. Nagaraja Rao, October 1987. (PB88-157169 A/S)

NESDIS 39 General Determination of Earth Surface Type and Cloud Amount Using Multispectral AVHRR Data. Irwin Ruff and Arnold Gruber, February 1988. (PB88-199195/AS)

NESDIS 40 The GOES I-M System Functional Description. Carolyn Bradley (Mitre Corp), November 1988.

NESDIS 41 Report of the Earth Radiation Budget Requirements Review - 1987 Rosslyn, Virginia, 30 March - 3 April 1987. L.L. Stowe (Editor), June 1988.

NESDIS 42 Simulation Studies of Improved Sounding Systems. H. Yates, D. Wark, H. Aumann, N. Evans, N. Phillips, J. Sussking, L. McMillin, A. Goldman, M. Chahine, and L. Crone, February 1989.

NESDIS 43 Adjustment of Microwave Spectral Radiances of the Earth to a Fixed Angle of Progagation. D. Q. Wark, December 1988. (PB89-162556/AS)

NESDIS 44 Educator's Guide for Building and Operating Environmental Satellite Receiving Stations. R. Joe Summers, Chambersburg Senior High, February 1989.

NESDIS 45 Final Report on the Modulation and EMC Considerations for the HRPT Transmission System in the Post NOAA-M Polar Orbiting Satellite ERA. James C. Fischer (Editor), June 1989. (PB89-223812/AS)

NESDIS 46 MECCA Program Documentation. Kurt W. Hess, September 1989.

NOAA SCIENTIFIC AND TECHNICAL PUBLICATIONS

The National Oceanic and Atmospheric Administration was established as part of the Departme Commerce on October 3, 1970. The mission responsibilities of NOAA are to assess the socioeconomic im of natural and technological changes in the environment and to monitor and predict the state of the Earth, the oceans and their living resources, the atmosphere, and the space environment of the Earth

The major components of NOAA regularly produce various types of scientific and technical info tion in the following kinds of publications:

PROFESSIONAL PAPERS—Important definitive research results, major techniques, and special investigations.

CONTRACT AND GRANT REPORTS—Reports prepared by contractors or grantees under NOAA sponsorship.

ATLAS—Presentation of analyzed data generally in the form of maps showing distribution of rainfall, chemical and physical conditions of oceans and atmosphere, distribution of fishes and marine mammals, ionospheric conditions, etc.

TECHNICAL SERVICE PUBLICATIONS—Reports containing data, observations, instructions, etc. A partial listing includes data serials; prediction and outlook periodicals; technical manuals, training papers, planning reports, and information serials; and miscellaneous technical publications.

TECHNICAL REPORTS—Journal quality with extensive details, mathematical developments, or data listings.

TECHNICAL MEMORANDUMS—Reports of preliminary, partial, or negative research or technology results, interim instructions, and the like.

U.S. DEPARTMENT OF COMMERCE
NATIONAL OCEANIC AND ATMOSPHERIC ADMINISTRATION
NATIONAL ENVIRONMENTAL SATELLITE, DATA, AND INFORMATION SERVICE
Washington, D.C. 20233